

Charge-state distribution of aerosolized nanoparticles

Jannik Lübke,^{1,2,3} Nils Roth,^{1,2} Lena Worbs,^{1,2} Daniel A. Horke,^{1,3, a)} Armando D. Estillore,¹ Amit K. Samanta,¹ and Jochen Küpper^{1,2,3, b)}

¹⁾ Center for Free-Electron Laser Science, Deutsches Elektronen-Synchrotron DESY, Notkestraße 85, 22607 Hamburg, Germany

²⁾ Department of Physics, Universität Hamburg, Luruper Chaussee 149, 22761 Hamburg, Germany

³⁾ Center for Ultrafast Imaging, Universität Hamburg, Luruper Chaussee 149, 22761 Hamburg, Germany

(Dated: 2021-08-11)

In single particle imaging experiments, beams of individual nanoparticles are exposed to intense pulses of x-rays from free-electron lasers to record diffraction patterns of single, isolated molecules. The reconstruction for structure determination relies on signal from many identical particles. Therefore, well-defined-sample delivery conditions are desired in order to achieve sample uniformity, including avoidance of charge polydispersity. We have observed charging of 220 nm polystyrene particles in an aerosol beam created by a gas-dynamic virtual nozzle focusing technique, without intentional charging of the nanoparticles. Here, we present a deflection method for detecting and characterizing the charge states of a beam of aerosolized nanoparticles. Our analysis of the observed charge-state distribution using optical light-sheet localization microscopy and quantitative particle trajectory simulations is consistent with previous descriptions of skewed charging probabilities of triboelectrically charged nanoparticles.

INTRODUCTION

Single particle imaging (SPI) experiments utilize x-ray diffractive imaging of individual nano-objects to determine their structure.^{1–3} On a shot-by-shot basis, a stream of aerosolized sample molecules e. g., artificial nanoparticles⁴ or biological macromolecules,⁵ is delivered into the focus of an FEL x-ray beam. The resulting diffraction patterns of the randomly oriented particles are collected and can subsequently be reconstructed into an average 3D volume with nanometer resolution.⁶ Careful and controlled sample delivery are key to successful SPI experiments:⁷ High-resolution structure reconstruction relies on a very large number of diffraction patterns of isolated, virtually identical particles.⁸

Biological macromolecules, like proteins, are intrinsically flexible⁹ and their structural integrity can be decreased by Coulomb repulsion between charges.¹⁰ Therefore, excessive charging of injected biomolecules during SPI experiments must be avoided to maintain their native structure. Neutralizing soft-x-ray sources¹¹ and careful aerosolization schemes^{12,13} help reduce charges on aerosols created with electrospray-ionization generators. For another popular atomization method using gas-dynamic virtual nozzles (GDVN),¹⁴ the gas-focused liquid jets are assumed to not actively charge the sample and buffer solution.¹⁵

Triboelectric charging of particles in the gas phase, i. e., after aerosolization, was characterized elsewhere.¹⁶ Although the possibility of triboelectric charging of nanoparticles in GDVNs was pointed out by some of us before,¹⁷

for these setups no detailed understanding of the process nor the extent of charging on individual nanoparticles is available. Here, we demonstrate a direct method for detecting and characterizing the charge-state distribution of a beam of aerosolized nanoparticles.

EXPERIMENTAL METHODS

In our experiment, prototypical polystyrene-sphere particles (Alfa Aesar, USA, $d = (220.0 \pm 17.6)$ nm) were transferred from aqueous suspension with a concentration of $7.5 \cdot 10^6$ particles/ml into the gas phase using a GDVN which consisted of a borosilicate glass capillary (inner diameter 30 μ m) fitted within a ceramic micro-injection-molded ejector tip.¹⁴ Liquid-sample-line flow rate of approximately 1 μ l/min with helium as sheath gas yielded a hit rate of six to seven particles per camera frame at 20 Hz frame rate, which allowed single-particle counting; acquisition of one data set took 500 s.

In the gas phase, excess helium was pumped away in a nozzle-skimmer stage¹⁸ and the particle beam was focused into the interaction region using an optimized¹⁹ aerodynamic-lens stack (ALS).^{20,21} We used an electrostatic deflector between the ALS exit and the detection position to disperse the initially cylindrically symmetric nanoparticle beam according to the particles' charges. The electric field was applied by two 70 mm long rod-shaped stainless-steel electrodes with a diameter of 4 mm and a center-point distance of 10 mm that were mounted $d_{\text{def}} = 14.7$ mm below the ALS exit using PEEK holders, see Fig. 1. The "+" electrode was connected to positive voltage of a power supply (Aim-TTi PLH250-P), whereas the "-" was connected to floating zero of the voltage supply. This created an inhomogeneous distorted two-wire field between the two electrodes and the grounded ALS. The steepest potential gradient between the rod electrodes

^{a)}Present address: Radboud University, Institute for Molecules and Materials, Heijendaalseweg 135, 6525 AJ Nijmegen, The Netherlands

^{b)}Email: jochen.kuepper@cfel.de; website: <https://www.controlled-molecule-imaging.org>

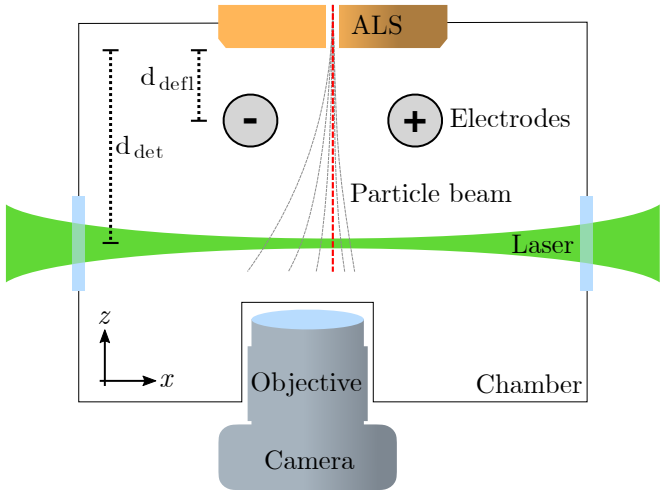


FIG. 1. **Experimental Setup.** A focused beam of aerosolized nanoparticles (red dashed line) is produced using an aerodynamic lens stack (ALS). The particles are deflected (grey dashed lines) by the inhomogeneous electric field between two rod-shaped electrodes centered in a plane at d_{defl} below the ALS. The nanoparticles were detected in a position-sensitive light-sheet microscopy setup at d_{det} below the ALS. The figure is not to scale, see text for details.

was 333.3 V/cm.

Individual particles were counted in a size- and position-sensitive light-scattering microscopy setup.^{22,23} The visible-light sheet for detection of the particles passed through the experimental chamber perpendicular to the injected particle beam $d_{\text{detect}} = 20$ mm below the last orifice of the ALS. We recorded the scattered light from intersecting particles using a microscope objective (5 \times , apochromatic long-working-distance infinity-corrected objective, Edmund Optics 59-876) and a sensitive camera (Teledyne Photometrics Prime 95b). The positions of the individual nanoparticles were accumulated into a two-dimensional (2D) position histogram, yielding a cross section through the particle beam at a given distance from the injector.

RESULTS AND DISCUSSION

Application of the light-sheet imaging method on the beam of polystyrene nanoparticles yielded the particle beam cross sections shown in Fig. 2. Without applying an electric field, a round particle-beam profile was observed with the highest density of particles in the center of the beam, Fig. 2 a. When applying the electric field the beam profile became highly asymmetric along the horizontal field direction, see Fig. 2 b. The majority of the particles were deflected to the left, i. e., away from the positive potential, directly implying a charge distribution of significant width and strongly skewed toward positive charges. These density profiles were integrated along the Y direction to yield the experimental beam profiles shown

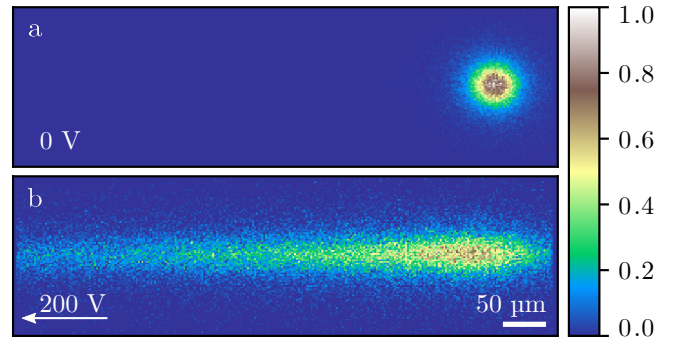


FIG. 2. **Particle-beam densities.** Particle-beam histograms at $d_{\text{detect}} = 20$ mm (a) without and (b) with an electric deflection field of 200 V applied. The white arrow indicates the electric-field direction. The colorbar is normalized to the highest counts in the 2D histograms.

in Fig. 3 (blue lines).

In order to model the observed profiles, we modeled this setup in SIMION²⁴ in 2D, approximating the experimental geometry using two circles for the electrodes and a rectangle for the injector tip, with the potentials fixed at a given voltage on the “+” electrode and 0 V on the “-” electrode and the ALS. The 2D approximation of the experimental setup in SIMION was appropriate, even though the particle beam was cylindrically symmetric

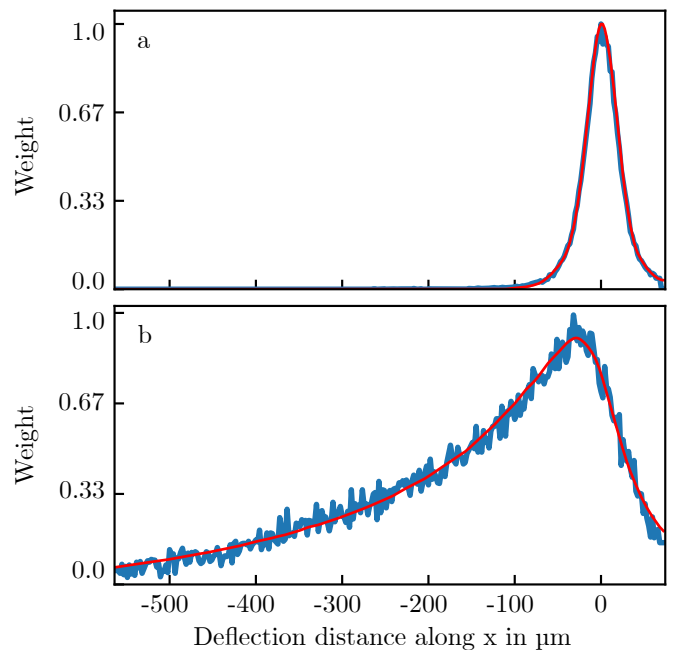


FIG. 3. **Measured and simulated particle-beam profiles.** One-dimensional particle-beam profiles for (a) 0 V and (b) 200 V, i. e., projections of the data in Fig. 2 onto the field axis (blue lines). Corresponding simulated particle-beam profiles (red lines) with all profiles normalized to the maximum number of events.

compared to translational symmetry of the electrostatic field: along Y , the field can be described as constant, because the rod electrodes are very long (70 mm) compared to the particle-beam dimensions (31.3 μm at $d_{\text{det}} = 20$ mm). So, for evaluating the particle deflection only the Z and X coordinates of the particles need to be considered. For a correct description of the electric far field the experimental chamber would also need to be modeled as another ground electrode, but this would only result in extensive simulation times and can be safely ignored based on our extensive experience.²⁵

Using the resulting electric field, we simulated the trajectories of sets of 32000 particles using a size distribution corresponding to the manufacturer's specifications ($d = (220 \pm 17.6)$ nm). Based on particle-beam 3D scans,²³ we could assume an initial particle-beam full-width-at-half-maximum (FWHM) of 56.2 μm at the ALS outlet and a width of 29.5 μm in the focus 18 mm below the ALS as well as nanoparticle speeds of $v = (130 \pm 15)$ m/s.

Elementary charges in the range $[-500, 500]$ were assigned to each set of particles and the respective 1001 individual-charge nanoparticle-density profiles were simulated. The simulated particle positions were sampled at $d_{\text{det}} = 20$ mm and collected into a histogram along X , yielding simulated line profile of the particle beams. We used a bin width of 1.85 μm , corresponding to the camera pixel edge length in the experimental microscopy setup.

We combined these individual-charge profiles into an overall nanoparticle-density profile as a weighted average to extract the charge-probability distribution of the nanoparticles. The weights, i.e., the contributions of the charge states to the sample, were determined from a fit to the experimental data. We used `scipy.optimize.differential_evolution`²⁶ with a maximum number of generations of 1000, a population size of 15, and a relative tolerance of convergence of 0.01 to minimize the mean squared error between the simulated and the measured profiles.

Models for describing the corresponding charge-state distribution included uniform, normal, and heavy-tailed – i.e., lognormal, loglogistic, scaled inverse Chi-squared, F, and normal-lognormal (NLN)²⁷ – distributions. NLN-distributed charge states were described elsewhere for triboelectrically charged microparticles.²⁸ In our case simulated particle-deflection beam profiles with NLN-distributed charges yielded highest agreement with experimental profiles. An NLN distribution can be described by the product of two sets of random variables, one being normally, the other lognormally distributed, which are referred to by three independent parameters. We fitted these parameters for the retrieval of an NLN distribution function that reproduced the experimental charge-state distribution very well.

We fitted the charge distribution of the particles in the beam to minimize the χ^2 deviation of experimental and simulated profiles of the particle beam along X . Optimization yielded the simulated profiles in Fig. 3 (red lines). We performed the corresponding χ^2 goodness-of-fit

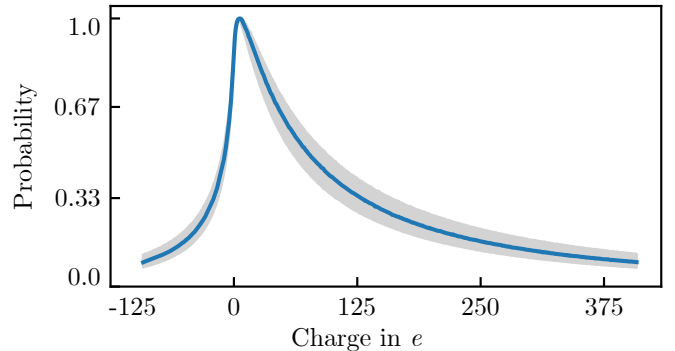


FIG. 4. **Charge-state distribution.** Histogram of the fitted charge-state distribution in the nanoparticle beam, normalized to the counts of the most probable charge of +5. The 1σ standard deviation in the probability is shown by the light gray area; see text for details.

test²⁹ with 160 degrees of freedom and a pre-determined level of significance $\alpha = 0.05$. We calculated p -values of $p > 0.99$. As $p > \alpha$ there is no significant difference between the measured data and simulations with the NLN-distributed charge states. Thus the underlying charge-state distribution of the measured particles can be adequately described by the obtained NLN distribution. The resulting nanoparticle-charge distribution is shown in Fig. 4. The most likely charge observed in our experiment is +5. The distribution shows a steep decrease toward smaller, i.e., negative, and a long tail of positive charges up to $>375 e$ on the 220 nm polystyrene latex spheres, corresponding to surface charge densities of up to $+39.5 \text{ nC cm}^{-2}$, which is reasonable (i.e., smaller) compared to published literature values³⁰ for positively charged polystyrene nanoparticles.

Positioning uncertainties of the experimental setup and possible deviation of the velocities of the particles were propagated through the simulations. Here, we assumed uncertainties for the positioning of the particle beam and the detection light-sheet in respect to the electrodes of $\pm 500 \mu\text{m}$. Furthermore, the mean initial particle-beam velocities were in the range $[120, 140]$ m/s to incorporate the uncertainty in the simulated velocity of the particles. These effects result in the uncertainties of the charge probability distribution in Fig. 4

These charges might originate from triboelectric charging in the GDVN,¹⁷ from collisions between nanoparticles, or in the aerosol transport tubes due to (multiple) collisions with the surrounding walls. Even though classical triboelectric charging models would suggest mainly negative charging of polystyrene on metal surfaces, deviations from the triboelectric series have been observed.^{31–34} Another source for particle charging might be the aerosolization process: during gas focusing of the liquid jet, the collision rates between gas molecules and sample droplets are high and charge transfer during this process can not be excluded. It is beyond the scope of the current work to fully determine these physical principles. Instead, we

provide a working tool for future studies when exploring these basics, possibly through systematic experiments about effects of sample material or aerosolization mechanisms, e.g., electrospray ionization or atomizers, on particle charging. The current results demonstrate the possibility for controlling and separating charged particles in SPI experiments and to investigate the effect of defined charges on overall sample structure and integrity.

CONCLUSION

In conclusion, we have demonstrated a method to characterize the charge-state distribution of a stream of aerosolized nanoparticles. An ALS injector was used to form a nanoparticle beam. When the beam was exposed to electrostatic field, we observed large deflection of the nanoparticles, indicating large charges. We have used charged-particle trajectory simulations to quantitatively describe our experimental setup. By iteratively fitting the simulated deflection profile with the experimental one, we have extracted the underlying charge-probability distribution, revealing significant positive charges ($>375 e$). Finding charges on GDVN-aerosolized particles is not necessarily intuitive. For example during SPI experiments, these particles are presumed to be overall neutral in charge.¹⁵ Excessive charging can be a source of structural variance of individual particles, and thus effectively a bottleneck for overall resolution in structure retrieval. If deemed necessary, neutralizing soft-x-ray devices may be employed to reduce the overall charges on the (GDVN-) aerosolized nanoparticles. In any case, during future SPI experiments, it would be highly beneficial to control or select the charge states of the aerosolized particles, e.g., using the electrostatic deflection technique we presented here.

ACKNOWLEDGMENTS

This work has been supported by Deutsches Elektronen-Synchrotron (DESY), a member of the Helmholtz Association (HGF), by the European Research Council under the European Union's Seventh Framework Program (FP7/2007-2013) through the Consolidator Grant COMOTION (614507), the Helmholtz Impuls und Vernetzungsfond, and the Cluster of Excellence "CUI: Advanced Imaging of Matter" of the Deutsche Forschungsgemeinschaft (DFG) (AIM, EXC 2056, ID 390715994).

- ¹R. Neutze, R. Wouts, D. van der Spoel, E. Weckert, and J. Hajdu, *Nature* **406**, 752 (2000).
- ²M. J. Bogan, W. H. Benner, S. Boutet, U. Rohner, M. Frank, A. Barty, M. M. Seibert, F. Maia, S. Marchesini, S. Bajt, B. Woods, V. Riot, S. P. Hau-Riege, M. Svenda, E. Marklund, E. Spiller, J. Hajdu, and H. N. Chapman, *Nano Lett.* **8**, 310 (2008).
- ³A. Barty, J. Küpper, and H. N. Chapman, *Annu. Rev. Phys. Chem.* **64**, 415 (2013).

- ⁴K. Ayyer, P. L. Xavier, J. Bielecki, Z. Shen, B. J. Daurer, A. K. Samanta, S. Awel, R. Bean, A. Barty, M. Bergemann, T. Ekeberg, A. D. Estillore, H. Fangohr, K. Giewekemeyer, M. S. Hunter, M. Karnevskiy, R. A. Kirian, H. Kirkwood, Y. Kim, J. Koliyadu, H. Lange, R. Letrun, J. Lübke, T. Michelat, A. J. Morgan, N. Roth, T. Sato, M. Sikorski, F. Schulz, J. C. H. Spence, P. Vagovic, T. Wollweber, L. Worbs, O. Yefanov, Y. Zhuang, F. R. N. C. Maia, D. A. Horke, J. Küpper, N. D. Loh, A. P. Mancuso, and H. N. Chapman, *Optica* **8**, 15 (2021), arXiv:2007.13597 [physics].
- ⁵A. Hosseinizadeh, G. Mashayekhi, J. Copperman, P. Schwander, A. Dashti, S. Sepehr, R. Fung, M. Schmidt, C. H. Yoon, B. G. Hogue, G. J. Williams, A. Aquila, and A. Ourmazd, *Nat. Meth.* **14**, 877 (2017).
- ⁶N.-T. D. Loh and V. Elser, *Phys. Rev. E* **80**, 026705 (2009).
- ⁷I. Martiel, H. M. Müller-Werkmeister, and A. E. Cohen, *Acta Cryst. D* **75**, 160 (2019).
- ⁸K. Ayyer, *Optica* **7**, 593 (2020), arXiv:2002.10267 [physics].
- ⁹X. Han, W.-H. Shin, C. W. Christoffer, G. Terashi, L. Monroe, and D. Kihara, in *Encyclopedia of Bioinformatics and Computational Biology*, edited by S. Ranganathan, M. Gribskov, K. Nakai, and C. Schönbach (Adv. Phys.) pp. 606–619.
- ¹⁰A. M. R. de Graff, M. J. Hazoglou, and K. A. Dill, *Structure* **24**, 329 (2016).
- ¹¹L. B. Modesto-Lopez, E. M. Kettleleson, and P. Biswas, *J. Electrostat.* **69**, 357 (2011).
- ¹²A. C. Leney and A. J. R. Heck, *J. Am. Soc. Mass. Spectrom.* **28**, 5 (2017).
- ¹³C. Santambrogio, A. Natalello, S. Brocca, E. Ponzini, and R. Grandori, *Proteomics* **19**, 1800060 (2018).
- ¹⁴K. R. Beyerlein, L. Adriano, M. Heymann, R. Kirian, J. Knoska, F. Wilde, H. N. Chapman, and S. Bajt, *Rev. Sci. Instrum.* **86**, 125104 (2015).
- ¹⁵D. P. DePonte, U. Weierstall, K. Schmidt, J. Warner, D. Starodub, J. C. H. Spence, and R. B. Doak, *J. Phys. D* **41**, 195505 (2008).
- ¹⁶M. Bierwirth, M. Gensch, and A. P. Weber, *Chem. Ing. Tech.* **93**, 1 (2021).
- ¹⁷S. Awel, R. A. Kirian, M. O. Wiedorn, K. R. Beyerlein, N. Roth, D. A. Horke, D. Oberthür, J. Knoska, V. Mariani, A. Morgan, L. Adriano, A. Tolstikova, P. L. Xavier, O. Yefanov, A. Aquila, A. Barty, S. Roy-Chowdhury, M. S. Hunter, D. James, J. S. Robinson, U. Weierstall, A. V. Rode, S. Bajt, J. Küpper, and H. N. Chapman, *J. Appl. Cryst.* **51**, 133 (2018), arXiv:1702.04014.
- ¹⁸N. Roth, S. Awel, D. A. Horke, and J. Küpper, *J. Aerosol. Sci.* **124**, 17 (2018), arXiv:1712.01795 [physics].
- ¹⁹L. Worbs, N. Roth, J. Lübke, A. Estillore, P. L. Xavier, A. K. Samanta, and J. Küpper, "Optimizing the geometry of aerodynamic lens injectors for single-particle coherent diffractive imaging of gold nanoparticles," (2021), submitted, arXiv:2105.15084v1 [physics].
- ²⁰P. Liu, P. J. Ziemann, D. B. Kittelson, and P. H. McMurry, *Aerosol Sci. Techn.* **22**, 293 (1995).
- ²¹N. Roth, D. Horke, J. Lübke, A. K. Samanta, A. Estillore, L. Worbs, N. Pohlman, K. Ayyer, A. Morgan, H. Fleckenstein, M. Domaracky, B. Erk, C. Passow, J. Correa, O. Yefanov, A. Barty, M. Prasciolu, S. Bajt, R. Kirian, H. Chapman, and J. Küpper, *Rev. Sci. Instrum.* (2021), submitted, arXiv:2012.11237 [physics].
- ²²S. Awel, R. A. Kirian, N. Eckerskorn, M. Wiedorn, D. A. Horke, A. V. Rode, J. Küpper, and H. N. Chapman, *Opt. Exp.* **24**, 6507 (2016), arXiv:1512.06231 [physics].
- ²³L. Worbs, J. Lübke, N. Roth, A. K. Samanta, D. A. Horke, and J. Küpper, *Opt. Exp.* **27**, 36580 (2019), arXiv:1909.08922 [physics].
- ²⁴Scientific Instrument Services Inc., USA, "Simion 8.1," (2011), URL: <http://simion.com>.
- ²⁵Y.-P. Chang, D. A. Horke, S. Trippel, and J. Küpper, *Int. Rev. Phys. Chem.* **34**, 557 (2015), arXiv:1505.05632 [physics].
- ²⁶P. Virtanen, R. Gommers, T. E. Oliphant, M. Haberland, T. Reddy, D. Cournapeau, E. Burovski, P. Peterson,

- W. Weckesser, J. Bright, S. J. van der Walt, M. Brett, J. Wilson, K. Jarrod Millman, N. Mayorov, A. R. J. Nelson, E. Jones, R. Kern, E. Larson, C. Carey, Í. Polat, Y. Feng, E. W. Moore, J. VanderPlas, D. Laxalde, J. Perktold, R. Cimrman, I. Henriksen, E. A. Quintero, C. R. Harris, A. M. Archibald, A. H. Ribeiro, F. Pedregosa, P. van Mulbregt, and SciPy 1.0 Contributors, *Nat. Meth.* **17**, 261 (2020).
- ²⁷M. Yang, *Appl. Econ. Lett.* **15**, 737 (2008).
- ²⁸J. Haerberle, A. Schella, M. Sperl, M. Schröter, and P. Born, *Soft Matter* **14**, 4987 (2018).
- ²⁹N. A. Heckert, J. J. Filliben, C. M. Croarkin, B. Hembree, W. F. Guthrie, P. Tobias, and J. Prins, *NIST/SEMATECH e-Handbook of Statistical Methods* (NIST, 2002) accessed 2020-12-16.
- ³⁰A. Fernández Barbero, R. Martínez García, M. A. Cabrerizo Vílchez, and R. Hidalgo-Alvarez, *Colloids Surf. A Physicochem. Eng. Asp.* **92**, 121 (1994).
- ³¹P. E. Shaw, *Nature* **118**, 659 (1926).
- ³²T. Shinbrot, T. S. Komatsu, and Q. Zhao, *Europhys. Lett.* **83**, 24004/p1 (2008).
- ³³R. Pham, R. C. Virnelson, R. M. Sankaran, and D. J. Lacks, *J. Electrostat.* **69**, 456 (2011).
- ³⁴C. Xu, B. Zhang, A. C. Wang, H. Zou, G. Liu, W. Ding, C. Wu, M. Ma, P. Feng, Z. Lin, and Z. L. Wang, *ACS Nano* **13**, 2034 (2019).